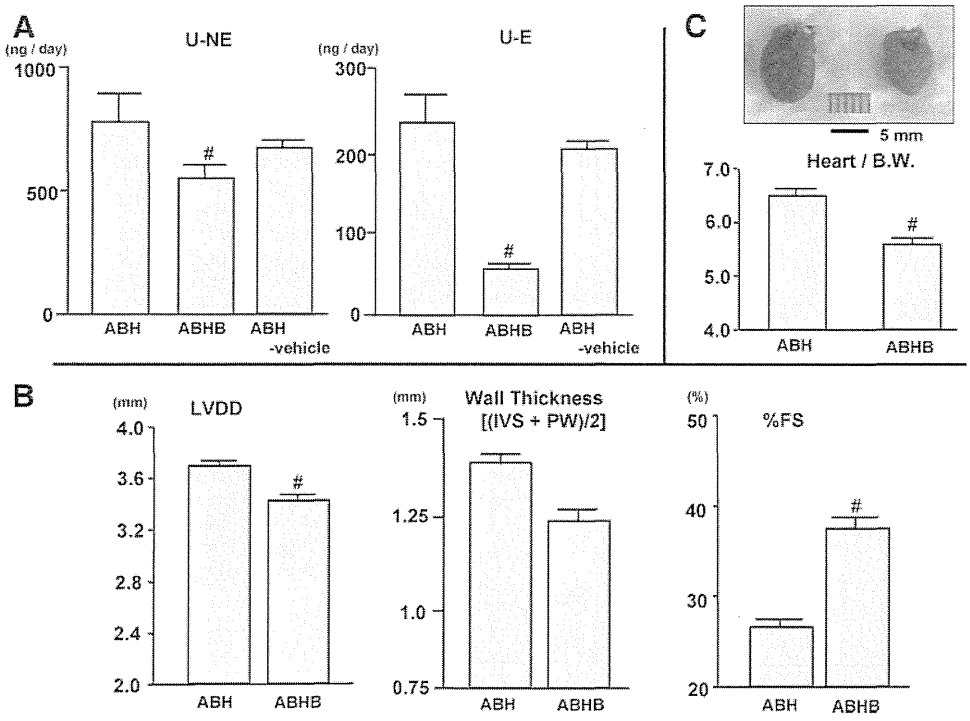

Figure 4. A, The 24-hour U-NE and U-E excretion in each group after ICV benzamil (AB-HB) infusion. #$P<0.05$ vs AB-H (n=5 to 10). B, Cardiac function evaluation by echocardiography in each group. IVS indicates interventricular septum; PW, posterior wall. #$P<0.05$ vs AB-H (n=8 in each group). C, Relative heart weight in each group. #$P<0.05$ vs AB-H (n=6 in each group).

101±5 mm Hg in regular-Na aCSF; n=4 for each). In Sham mice, high-Na aCSF ICV infusion had no significant effects on cardiac function compared with regular-Na aCSF ICV infusion (LVDD, 3.1±0.2 mm in high-Na aCSF versus 3.1±0.3 mm in regular-Na aCSF; %FS, 46±2% in high-Na aCSF versus 48±3% in regular-Na aCSF; n=5 for each).

Effects of ENaC Blocker ICV Infusion on Cardiac Function

In comparison with AB-H mice, ICV infusion of the ENaC blocker benzamil (AB-HB mice) significantly decreased U-NE and U-E excretion (Figure 4A). Cardiac function (LVDD and %FS) significantly improved in AB-HB mice compared with AB-H mice (Figure 4B). Relative heart weight decreased in AB-HB mice compared with AB-H mice (Figure 4C). Arterial pressure was significantly higher and heart rate was lower in AB-HB mice than in AB-H mice (Online Table II). ICV infusion of benzamil did not affect these measures in AB-R mice, and ICV infusion of vehicle in AB-H mice also did not significantly decrease U-NE and U-E excretion (data not shown).

Rho-Kinase Activity and AT_1R Expression in the Brain

The amount of AT_1R and the expression of p-moesin, a substrate of Rho-kinase, in the brain stem and circumventricular tissue were significantly higher in AB-4 mice than in Sham-4 mice (Figure 5).

Effects of ICV Infusion of Rho-Kinase Inhibitor and AT_1R Blocker on Cardiac Function

In comparison with AB-H mice, ICV infusion of the Rho-kinase inhibitor Y-27632 (AB-HY mice) or AT_1R blocker telmisartan (AB-HT mice) induced a significant decrease in U-NE and U-E excretion (Figure 6A). In AB-HT mice, U-NE and U-E decreased in a dose-related manner. Cardiac function was also significantly improved in AB-HY mice or AB-HT mice compared with AB-H mice (Figure 6B). Relative heart weight was decreased in AB-HY mice or AB-HT mice compared with AB-H mice (Figure 6C). Heart rate was significantly decreased in AB-HY mice or AB-HT mice compared with AB-H mice (Online Table II). Infusion of vehicle (aCSF or DMSO) did not have these effects.

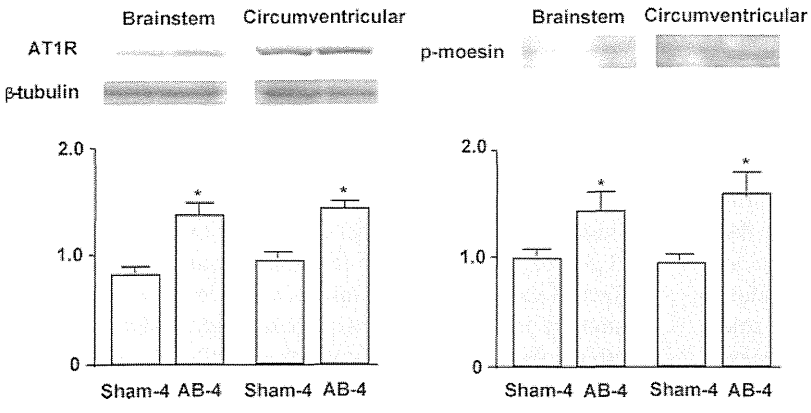

Figure 5. Left, Representative Western blots demonstrating the expression of AT_1R in the brain (circumventricular tissues including hypothalamus and brain stem tissues) of Sham-4 or AB-4. The graph shows the means for the quantification of 4 separate experiments. Data are expressed as the relative ratio to β-tubulin expression (n=4 in each group). *$P<0.05$ vs Sham-4. Right, Representative Western blot demonstrating the expression of p-moesin, a substrate of Rho-kinase in the brain (circumventricular tissues including hypothalamus and brain stem tissues) of Sham-4 or AB-4. The graph shows the means for the quantification of 3 separate experiments. Data are expressed as the relative ratio to Sham-4, which was assigned a value of 1 (n=3 in each group). *$P<0.05$ vs Sham.

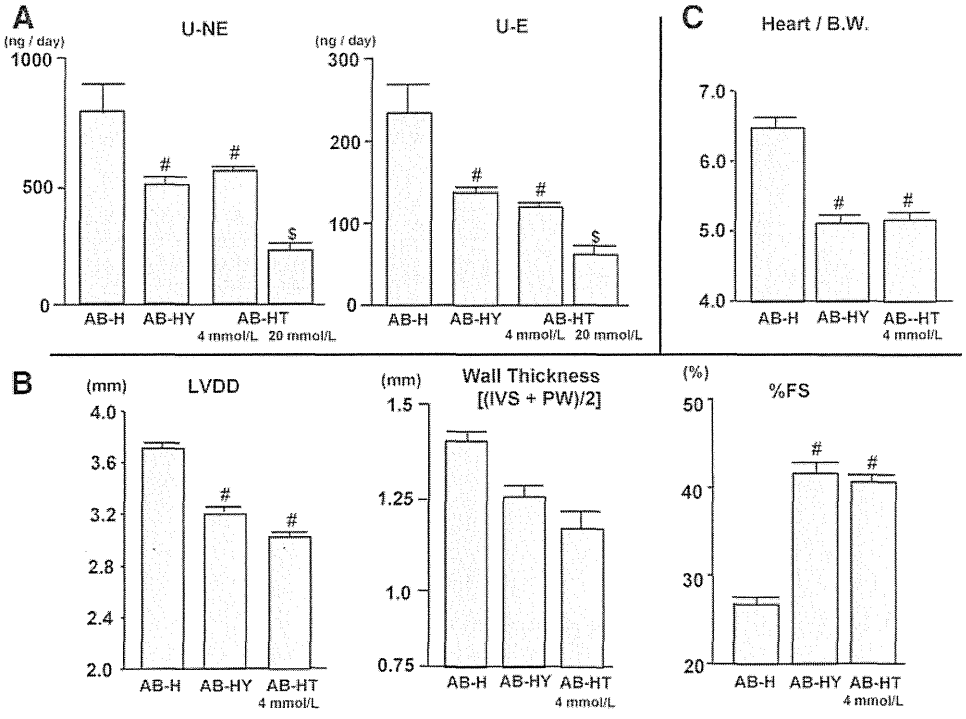

Figure 6. A, The 24-hour U-NE and U-E excretion in each group after Y-27632 (AB-HY) or telmisartan (AB-HT) ICV infusion. #$P<0.05$ vs AB-H (n=5 to 10), \$$P<0.05$ vs AB-HT 4 mmol/L. B, Cardiac function evaluation by echocardiography in each group after Y-27632 (AB-HY) or telmisartan (AB-HT) ICV infusion. IVS indicates interventricular septum; PW, posterior wall. #$P<0.05$ vs AB-H (n=5 to 8). C, Relative heart weight in each group after Y-27632 (AB-HY) or telmisartan (AB-HT) ICV infusion. #$P<0.05$ vs AB-H (n=5 to 6).

Serum Parameters

Serum Na concentration did not differ between groups (Sham-4, 151±2 mEq/L; AB-4, 151±1 mEq/L; AB-R, 150±1 mEq/L; AB-H, 152±1 mEq/L). Serum creatinine concentration, as a marker of renal function, also did not differ between groups (Sham-4, 0.11±0.01 mg/dL; AB-4, 0.09±0.01 mg/dL; AB-R, 0.12±0.01 mg/dL; AB-H, 0.11±0.01 mg/dL). Serum aldosterone levels were not different between Sham-4 and AB-4 mice and were significantly lower in AB-H mice than in AB-4 mice, AB-R mice, and Sham-4 mice (Sham-4, 120±11 pg/dL; AB-4, 145±28 pg/dL; AB-R, 163±17 pg/dL; AB-H, 54±6 pg/dL; n=6 to 7; $P<0.05$).

Discussion

The major findings of the present study were that mice with pressure overload produced by aortic banding acquired brain Na sensitivity via the activation of brain ENaCs through stimulation of the Rho/Rho-kinase pathway and RAS. Because of the acquired brain Na sensitivity, high salt intake led to sympathetic activation, which led to the deterioration of cardiac function. These findings are novel and suggest new targets for studies of the prevention and treatment of cardiac deterioration in patients with pressure overload, such as hypertensive heart disease.

The most important finding of the present study was that the mice with pressure overload acquired brain Na sensitivity and a high-salt diet increased the sympathetic outflow before cardiac dysfunction was detected. In AB-4 mice, only LVWT tended to increase compared to the Sham-4 mice, but there was no effect on cardiac function. Both a high-salt and regular-salt diet for an additional 4 weeks, however, induced cardiac dysfunction in AB mice compared with Sham mice. Furthermore, AB mice on the high-salt diet exhibited significantly more severe cardiac dysfunction and greater activation of the sympathetic system than AB mice on the regular-salt diet. This high-salt induced enhanced sympathetic drive was obvious before cardiac function was impaired. In Sham mice, a high salt intake did not increase U-NE and U-E excretion and had no effect on cardiac function. These results strongly suggest that the mice with pressure overload acquired the salt sensitivity before cardiac function began to deteriorate and that a high salt intake augmented cardiac dysfunction by inducing sympathetic activation.

To clarify the contribution of central mechanisms to the acquisition of salt sensitivity in mice with pressure overload, we examined the effects of high-Na in the CSF on sympathetic activity and arterial pressure after ICV infusion of high-Na or regular-Na aCSF. Compared with ICV infusion of regular-Na aCSF, high-Na aCSF induced significant increases in U-NE and U-E excretion in both groups of mice. The increased U-NE excretion in AB mice, however, tended to be greater than that in Sham mice ($P=0.1$), and the increase in U-E excretion was significantly greater in AB mice than in Sham mice. Furthermore, ICV infusion of high-Na aCSF induced significantly greater increases in arterial pressure and heart rate in AB-4 mice than in Sham-4 mice. To assess the specificity of the pressure response to a high-Na ICV infusion, we examined the response to other central stimuli, such as angiotensin II and carbachol. The response to angiotensin II was greater in AB-4 mice than Sham-4 mice. In contrast, the response to carbachol was not different between groups. The effect of the angiotensin II ICV infusion was supported by the findings that the extent of brain AT_1R was greater in AB-4 mice than Sham-4 mice, and the effect of carbachol ICV infusion indicated the specific activation of the brain RAS and Na sensing system. Together with the findings from the systemic salt loading, our findings suggest that the acquisition of Na sensitivity in the brain of

mice with pressure overload results from two different mechanisms: (1) the enhancement of Na uptake into the brain and (2) the increase in responsiveness to Na within the brain.

Another important finding of the present study was the high-Na aCSF-induced activation of the sympathetic system, which further deteriorates cardiac function in mice with pressure overload. There are some reports that enhanced sympathetic drive plays an important role in the progression of heart failure.[20,21] In the present study, in comparison with ICV infusion of regular-Na aCSF, high-Na aCSF induced a significant decline in cardiac function. To evaluate the possibility that the increase in the afterload induced by increased arterial pressure affected cardiac function, we measured arterial pressure 2 weeks after ICV infusion of high-Na aCSF and confirmed that arterial pressure did not significantly increase compared with regular-Na ICV infusion. These results suggest that high-Na aCSF-induced sympathetic hyperactivation may lead to cardiac dysfunction in mice with pressure overload and the deterioration of cardiac function may not be attributable to the increase in the afterload induced by the arterial pressure elevation. However, high-salt loading caused further decreases in cardiac function in AB mice, indicating that high-salt loading may induce further decrease in cardiac function both by sympathetic activation and an increase in arterial pressure in AB mice.

Arterial pressure in AB-4 mice was significantly higher than that in Sham-4 mice; and arterial pressure in AB-H 1-week mice, which were loaded with a high-salt diet for 1 week, was further increased compared with that in AB-4 mice. Arterial pressure in AB-R mice and AB-H mice decreased to levels similar or lower than that in Sham mice within 8 weeks. This may relate to cardiac dysfunction. In fact, the LVEDP in AB-H mice was significantly greater than that in AB-R or Sham-R mice and the LV %FS in AB-H mice was significantly smaller than that in AB-R or Sham-R mice. To validate the arterial pressure measurements, we measured arterial pressure and heart rate using a radio-telemetry system with mice in the awake state. At day 28 after aortic banding (AB-4 mice), arterial pressure was significantly higher than that before aortic banding. Thereafter, in AB-H mice, arterial pressure was significantly further increased at day 35 (1 week after the starting high-salt diet), but the general health of the mice deteriorated, likely because of severe lung congestion, which was supported by the high lung/body weight ratio. In AB-R mice, arterial pressure peaked at around day 40 and then gradually decreased. Implantation of the telemetry catheter in the carotid artery might further augment the pressure overload and induce severe lung congestion in AB-H mice. Therefore, we examined the arterial pressure under anesthesia in acute experiments. The findings indicate that aortic banding causes a pressure overload for LV and high-salt loading superimposed on aortic banding further augments the pressure overload.

To explore the mechanisms of the acquisition of brain Na sensitivity, we examined the effects of an ENaC blocker, benzamil. Brain ENaCs are involved in the high salt–induced increase in central sympathetic outflow in salt-sensitive hypertensive rats.[1,3] In the present study, brain ENaC blockade by benzamil attenuated the high salt–induced activation of the sympathetic nervous system and the deterioration of cardiac function. Furthermore, we examined the brain Na concentrations in each group. We were unable to measure Na concentrations in the CSF in the present study, because in mice it is difficult to obtain the volume of CSF required to measure Na concentration. Therefore, we measured the Na concentrations in the brain tissues and confirmed that AB-H mice had higher Na concentrations than the other groups. These findings support our hypothesis that the pressure overload activates brain ENaCs and augments Na transport from plasma to the CSF, resulting in sympathoexcitation. However, we did not examine the effects of brain ENaCs on Na transport directly and ENaCs have both epithelial and neural components.[11] Therefore, it is possible that the benzamil may affect ENaCs on neural components and cause sympathoinhibitory effects. The role of ENaCs on neural components in sympathetic modulation remains unclear. A similar dose of benzamil was used as specific ENaC blocker in previous studies,[4] and the estimated benzamil concentration in the CSF in the present study was considered to be specific for ENaCs (<100 nmol/L).[22–24] Therefore, the dose of benzamil used in the present study was adequate for use as a specific ENaC blocker. Further studies are required to measure ENaC activity directly. Although some studies have demonstrated that salt intake induces sympathoexcitation via central mechanisms[1–3] and the effects of brain ENaCs on cardiac function,[4] these previous studies used genetic models of salt-sensitive hypertension or heart failure induced by myocardial infarction, whereas we used the pressure overload produced by aortic banding model in mice without a genetic background of salt sensitivity.

Finally, we focused on Rho-kinase and angiotensin II as the mechanisms involved in brain ENaC activation in the mice with pressure overload, because ENaCs in kidney are reported to be activated by Rho-kinase[12] and angiotensin II.[13] In addition, we recently reported that Rho-kinase[16,25–27] and angiotensin II[28] in the brain contribute to cardiovascular regulation via the sympathetic nervous system. In the present study, we confirmed that compared to Sham-4 mice, the brains of AB-4 mice had higher levels of AT_1R and higher Rho-kinase activity, and blockade of either AT_1R or Rho-kinase attenuates high salt–induced sympathetic activation and cardiac dysfunction. These findings suggest that enhanced brain Na sensitivity results from the activation of brain ENaCs via the Rho/Rho-kinase pathway and RAS in mice with pressure overload. However, ENaCs may be upstream of RAS in brain.[29] In the present study, we did not address this issue. Further studies are needed to clarify the relationship between RAS and ENaCs in brain. It is possible that renal blood flow is reduced in mice with suprarenal abdominal aortic banding, resulting in renal dysfunction[30] concomitant with activation of the systemic RAS.[31] It is unlikely that this occurred in the present study because we confirmed that serum creatinine and aldosterone levels were not significantly different between groups and the mean arterial pressure in the AB-4 mice measured from the right femoral artery was above 90 mm Hg, suggesting that the aortic banding procedure did not significantly reduce renal blood flow and impair renal function. Previous studies

demonstrated that excess stimulation of cardiopulmonary and arterial baroreceptors impair baroreflex function[32,33] and RAS[32] or Rho-kinase[33] in the brain might contribute to the impaired baroreflex function. In the present study, we demonstrated that arterial pressure measured from the carotid artery and LVEDP were significantly greater in AB-4 mice than in Sham-4 mice. The excess stimulation of cardiopulmonary and arterial baroreceptor may contribute to the activation of the Rho/Rho-kinase pathway and RAS in the brains of the mice with pressure overload, even before high-salt loading.

In conclusion, the present findings strongly suggest that mice with pressure overload acquire brain Na sensitivity because of the activation of brain ENaCs via the Rho/Rho-kinase pathway and RAS. The acquired brain Na sensitivity contributes to high salt–induced sympathetic activation, leading to deteriorating cardiac function in mice with pressure overload.

Sources of Funding

This work was supported by Grants-in-Aid for Scientific Research from the Japan Society for the Promotion of Science (B19390231 and 19890148) and the Mitsubishi Pharma Research Foundation.

Disclosures

None.

References

1. Nishimura M, Ohtsuka K, Nanbu A, Takahashi H, Yoshimura M. Benzamil blockade of brain Na^+ channels averts Na^+-induced hypertension in rats. *Am J Physiol.* 1998;274:R635–R644.
2. Fujita M, Ando K, Nagae A, Fujita T. Sympathoexcitation by oxidative stress in the brain mediates arterial pressure elevation in salt-sensitive hypertension. *Hypertension.* 2007;50:360–367.
3. Huang BS, Amin MS, Leenen FHH. The central role of the brain in salt-sensitive hypertension. *Curr Opin Cardiol.* 2006;21:295–304.
4. Huang BS, Leenen FHH. Blockade of brain mineralcorticoid receptors or Na^+ channels prevents sympathetic hyperactivity and improve cardiac function in rats post-MI. *Am J Physiol.* 2005;288:H2491–H2497.
5. Leenen FHH. Brain mechanisms contributing to sympathetic hyperactivity and heart failure. *Circ Res.* 2007;101:221–223.
6. Mark AL. Sympathetic dysregulation in heart failure: mechanisms and therapy. *Clin Cardiol.* 1995;18:I3–I8.
7. Zucker IH. Novel mechanisms of sympathetic regulation in chronic heart failure. *Hypertension.* 2006;48:1005–1011.
8. Takimoto E, Champion HC, Li M, Belardi D, Ren S, Rodriguez ER, Bedja D, Gabrielson KL, Wang Y, Kass DA. Chronic inhibition of cyclic phosphodiesterase 5A prevents and reverse cardiac hypertrophy. *Nat Med.* 2005;11:214–222.
9. Klotz S, Hay I, Zhang G, Maurer M, Wang J, Burkhoff D. Development of heart failure in chronic hypertensive Dahl rats focus on heart failure with preserved ejection fraction. *Hypertension.* 2006;47:901–911.
10. Vigne P, Champigny G, Marsaut R, Barbry P, Frelin C, Lazdunski M. A new type of amiloride-sensitive cation channel in endothelial cells of brain microvessels. *J Biol Chem.* 1989;264:7663–7668.
11. Amin MS, Wang HW, Reza E, Whitman SC, Tuana BS, Leenen FHH. Distribution of epithelial sodium channels and mineralocorticoid receptors in cardiovascular regulatory centers in rat brain. *Am J Physiol.* 2005;289:R1787–R1797.
12. Pochynyuk O, Medina J, Gamper N, Genth H, Stockand JD, Staruschenko A. Rapid translocation and insertion of the epithelial Na^+ channel in response to RhoA signaling. *J Biol Chem.* 2006;281:26520–26527.
13. Peti-Peterdi J, Warnock DG, Bell PD. Angiotensin II directly stimulates ENaC activity in the cortical collecting duct via AT1 receptors. *J Am Soc Nephrol.* 2002;13:1131–1135.
14. Harada K, Komuro I, Shiojima I, Hayashi D, Kudoh S, Mizuno T, Kijima K, Matsubara H, Sugaya T, Murakami K, Yazaki Y. Pressure overload induces cardiac hypertrophy in angiotensin II type II 1A receptor knockout mice. *Circulation.* 1998;97:1952–1959.
15. Sakai K, Hirooka Y, Shigematsu H, Kishi T, Ito K, Shimokawa H, Takeshita A, Sunagawa K. Overexpression of eNOS in brain stem reduces enhanced sympathetic drive in mice with myocardial infarction. *Am J Physiol Heart Circ Physiol.* 2005;289:H2159–H2166.
16. Ito K, Kimura Y, Hirooka Y, Sagara Y, Sunagawa K. Activation of Rho-kinase in the brainstem enhances sympathetic drive in mice with heart failure. *Auton Neurosci.* 2008;142:77–81.
17. Wirth A, Benyó Z, Lukasova M, Leutgeb B, Wettschureck N, Gorbey S, Örsy P, Horváth B, Maser-Gluth C, Greiner E, Lemmer B, Schütz G, Gutkind S, Offermanns S. G_{12}-G_{13}-LARG-mediated signaling in vascular smooth muscle is required for salt-induced hypertension. *Nat Med.* 2008;14:64–68.
18. Uehata M, Ishizaki T, Satoh H, Ono T, Kawahara T, Morishita T, Tamakawa H, Yamagami K, Inui J, Maekawa M, Narumiya S. Calcium sensitization of smooth muscle mediated by a Rho-associated protein kinase in hypertension. *Nature.* 1997;389:990–994.
19. Matsui T, Maeda M, Doi Y, Yonemura S, Amano M, Kaibuchi K, Tsukita S. Rho-kinase phosphorylate COOH-terminal threonines of ezrin/radixin/moesin (ERM) proteins and regulates their head-to-tail association. *J Cell Biol.* 1998;140:647–657.
20. Cohn JN, Levine TB, Olivari MT, Garberg V, Lura D, Francis GS, Simon AB, Rector T. Plasma norepinephrine as a guide to prognosis in patients with chronic congestive heart failure. *N Engl J Med.* 1984;311:819–823.
21. Rector TS, Olivari MT, Levine TB, Francis GS, Cohn JN. Predicting survival for an individual with congestive heart failure using the plasma norepinephrine concentration. *Am Heart J.* 1987;114:148–152.
22. Teiwes J, Toto RD. Epithelial sodium channel inhibition in cardiovascular disease. *Am J Hypertens.* 2007;20:109–117.
23. Hirsh AJ, Sabater JR, Zamurs A, Smith RT, Paradiso AM, Hopkins S, Abraham WM, Boucher RC. Evaluation of second generation amiloride analogs as therapy for cystic fibrosis lung disease. *J Pharmacol Exp Ther.* 2004;311:929–938.
24. Rudick RA, Zirretta DK, Herndon RM. Clearance of albumin from mouse subarachnoid space: a measure of CSF bulk flow. *J Neurosci Methods.* 1982;6:253–259.
25. Ito K, Hirooka Y, Sakai K, Kishi T, Kaibuchi K, Shimokawa H, Takeshita A. Rho/Rho-kinase pathway in brain stem contributes to blood pressure regulation via sympathetic nervous system: possible involvement in neural mechanisms of hypertension. *Circ Res.* 2003;92:1337–1343.
26. Ito K, Hirooka Y, Kishi T, Kimura Y, Kaibuchi K, Shimokawa H, Takeshita A. Rho/Rho-kinase pathway in the brainstem contributes to hypertension caused by chronic nitric oxide synthase inhibition. *Hypertension.* 2004;43:156–162.
27. Ito K, Hirooka Y, Kimura Y, Sagara Y, Sunagawa K. Ovariectomy augments hypertension through Rho-kinase activation in the brain stem in female spontaneously hypertensive rats. *Hypertension.* 2006;48:651–657.
28. Sagara Y, Hirooka Y, Nozoe M, Ito K, Kimura Y, Sunagawa K. Pressor response induced by central angiotensin II is mediated by activation of Rho/Rho-kinase pathway via AT_1 receptors. *J Hypertens.* 2007;25:399–406.
29. Huang BS, Cheung WJ, Wang Hao, Tan J, White RA, Leenen FHH. Activation of brain renin-angiotensin-aldosterone system by central sodium in Wister rats. *Am J Physiol.* 2006;291:H1109–H1117.
30. Akers WS, Cross A, Speth R, Dwoskin LP, Cassis LA. Renin-angiotensin system andsympathetic nervous system in cardiac pressure-overload hypertrophy. *Am J Physiol.* 2000;279:H2797–H2806.
31. Héliés-Toussaint C, Moinard C, Rasmusen C, Tabbi-Anneni I, Cynober L, Gryngerg A. Aortic banding in rats as a model to investigate malnutrition associated with heart failure. *Am J Physiol.* 2005;288:R1325–R1331.
32. Wang WZ, Gao L, Pan YX, Zucker IH, Wang W. AT1 receptor in the nucleus tractus solitarii mediate the interaction between the baroreflex and the cardiac sympathetic afferent reflex in anesthetized rats. *Am J Physiol.* 2007;292:R1137–R1145.
33. Ito K, Hirooka Y, Sagara Y, Kimura Y, Kaibuchi K, Shimokawa H, Takeshita A, Sunagawa K. Inhibition of Rho-kinase in the brainstem augments baroreflex control of heart rate in rats. *Hypertension.* 2004;44:478–483.

Online Data Supplement

Expanded Materials and Methods

Animals

The study was reviewed and approved by the Committee on Ethics of Animal Experiments, Kyushu University Graduate School of Medical Sciences, and conducted according to the Guidelines for Animal Experiments of Kyushu University. Male Institute of Cancer Research (ICR) mice (10 weeks old; SLC, Fukuoka, Japan) were used.

Mouse LVH Model Preparation

The suprarenal abdominal aorta[1] was banded in mice (AB mice) under sodium pentobarbital (25–40 mg/kg i.p.) anesthesia. The abdominal aorta was constricted at the suprarenal level with 5-0 silk sutures guided by a blunted 27-gauge needle, which was withdrawn as quickly as possible. Sham-operated (Sham) mice served as controls. Four weeks later, AB and Sham mice were each divided into 2 groups: 1) mice fed a high-salt (8% NaCl) diet for 4 weeks (AB-H mice and Sham-H mice) and 2) mice fed a regular-salt (0.3% NaCl) diet for 4 weeks (AB-R mice and Sham-R mice; Figure 1; protocol-1).

Evaluation of Cardiac Function

Cardiac function was evaluated by echocardiography.[2,3] Serial M-mode echocardiography was performed on mice under light sodium pentobarbital anesthesia with spontaneous respiration. An echocardiography system (SSD5000; Aloka, Tokyo, Japan) with a dynamically focused 7.5-MHz linear array transducer was used. M-mode tracings were recorded from the short-axis view at the

level of the papillary muscle. Left ventricle (LV) end-diastolic diameter (LVDD), LV end-systolic diameter (LVSD), and LV wall thickness (LVWT) were measured. LVWT was calculated as the average of the thickness of the interventricular septum and the posterior LV wall. Percent fractional shortening (%FS) was calculated as follows: %FS = (LVDD) − (LVSD) / (LVDD) × 100. Cardiac function was also evaluated by LV End-Diastolic Pressure (LVEDP). LVEDP was measured with a conductance catheter (1.4 Fr; Miller Instruments®) inserted into the right carotid artery and advanced across the aortic valve into the left ventricle.

Measurement of Arterial Pressure and Heart Rate

Under sodium pentobarbital anesthesia (25–40 mg/kg i.p.), mice were intubated using a 20-gauge soft catheter and ventilated with a tidal volume of 1.0-1.5 mL at 120 cycles/min with the fraction of inspired oxygen equal to 0.21.[2,4] A catheter was then inserted into the right carotid artery to measure arterial pressure and heart rate. In another protocol, arterial pressure and heart rate were measured in awake AB-H and AB-R mice using a radio-telemetry system (Data Sciences International).[5] Under sodium pentobarbital anesthesia (25–40 mg/kg i.p.), the telemetry catheter was implanted into the left carotid artery and the transducer unit was inserted into a subcutaneous pouch along the abdomen. Each mouse was housed in an individual cage after operation and unrestricted and free move in their cage. The case was placed over the receiver panel connected to the computer for data acquisition. Arterial pressure and heart rate were recorded continuously for 5 minutes and averaged.

Evaluation of Sympathetic Activity

Sympathetic activity was evaluated by measuring 24-h urinary norepinephrine (U-NE) and urinary epinephrine (U-E) excretion using high-performance liquid chromatography.[2,4]

Evaluation of Na Sensitivity

U-NE and U-E after high salt intake was compared between Sham mice and AB mice. Four weeks after AB (AB-4 mice) or sham operation (Sham-4 mice), mice were fed a high-salt (8% NaCl) diet. Five days after starting the high-salt diet, 24-h U-NE and U-E excretion were measured, and echocardiography was performed to confirm that cardiac function was preserved. In addition, U-NE and U-E excretion in response to high-Na (0.2 mol/L) aCSF ICV infusion (0.25 L/h for 14 days, using an osmotic minipump) were measured in Sham mice and AB mice. Under anesthesia with sodium pentobarbital (25–40 mg/kg i.p.), mice were placed on a stereotaxic frame. The skin overlying the midline of the skull was incised, and a small hole with the following coordinates was bored using a dental drill: 0.3 mm posterior and 1 mm lateral relative to the bregma, and 3 mm ventral to the skull surface.[6] An Alzet® brain infusion kit 3 (DURECT Corporation, CA) connected to an osmotic minipump (Alzet model 1004; DURECT) was fixed to the skull surface with tissue adhesive. The pump was inserted subcutaneously on the back. Mice with ICV infusion of regular-Na (0.145 mol/L) aCSF served as the controls (R-Na ICV-mice; Figure 1; protocol-2). Before and 2 weeks after starting the ICV infusion, sympathetic activity, cardiac function, arterial pressure, and heart rate were measured by the methods described above.

The effects of high-Na (0.2 mol/L) aCSF ICV infusion on arterial pressure and heart rate were also evaluated in Sham-4 mice and AB-4 mice in acute experiments. Arterial pressure and heart rate were measured via a catheter in the right carotid artery under anesthesia. High-Na (0.2 mol/L) aCSF was infused ICV with a microsyringe pump (infusion rate: 1 L/min for 10 min) and changes in arterial pressure and heart rate were measured. Furthermore, the effects of other central stimuli, such as angiotensin II or carbachol ICV infusion on arterial pressure were

examined. Angiotensin II (Sigma) (0.5 nmol/L, 1 L/min for 5 min) or carbachol (Sigma) (0.1 mmol/L, 1 L/min for 5 min) was infused. The dose of each chemical was also determined according to the previous reports.[7,8]

Measurement of Brain Na Concentration

Under anesthesia with an overdose of sodium pentobarbital, the mice were perfused with dH_2O. After adequate perfusion to remove blood, the brain circumventricular tissues and hypothalamus were dissected out. The tissues (0.10 ± 0.01 g) were homogenized in 200 L of dH_2O, centrifuged, and the supernatant was collected. The Na concentration in each sample was measured.

Measurement of Organ Weight

After completion of the experiments, mice were killed with an overdose of sodium pentobarbital, and the heart and lungs were removed and weighed.

Measurement of Serum Parameters

Within minutes after the mice were injected with an overdose of sodium pentobarbital, a blood sample was collected from the right ventricle and rapidly centrifuged (6000 rpm for 10 min). The obtained serum sample was then stored at −20°C before measuring serum components. We evaluated the aldosterone concentration by radioimmunoassay, Na concentration by electrode methods, and creatinine by enzymatic methods.

Evaluation of the Effects of Na-Channel Blockade in the Brain

Benzamil (Sigma), a specific epithelial Na-channel (ENaC) blocker[9] (1 mg/mL, dissolved in

aCSF), was infused ICV in AB-H mice (AB-HB mice) and AB-R mice (AB-RB mice) using an osmotic minipump (0.11 L/h for 4 weeks). Four weeks later, 24-h U-NE and U-E excretion, arterial pressure, heart rate, and organ weight were measured, and echocardiography was performed as described earlier. Mice with ICV infusion of only aCSF (vehicle) served as controls (aCSF mice; Figure 1; protocol-1).

Evaluation of the Effects of Rho-Kinase and Angiotensin Type 1 Receptors (AT1R) Blockade in the Brain

A specific Rho-kinase inhibitor, Y-27632[10] (Calbiochem, 5 mmol/L, dissolved in aCSF), or an AT1R blocker, telmisartan (Sigma, 4 mmol/L, 20 mmol/L, dissolved in demethyl sulfoxide [DMSO]) was infused ICV in ABH mice (AB-HY or AB-HT mice, respectively) using an osmotic minipump (0.11 L/h for 4 weeks). Four weeks later, 24-h U-NE/U-E excretion, arterial pressure, heart rate, and organ weight were measured; echocardiography was performed in AB-HY mice and AB-HT mice as described earlier (Figure 1; protocol-1).

Evaluation of AT1R Expression and Rho-Kinase Activity

The animals were killed with an overdose of sodium pentobarbital, and circumventricular tissues including the hypothalamus and brainstem tissues were obtained. The tissues were homogenized in a lysing buffer containing 40 mmol/L HEPES (4-[2-hydroxyethyl]-1-piperazineethanesulfonic acid), 1% Triton® X-100, 10% glycerol, 1 mmol/L Na_3VO_4 (sodium orthovanadate), and 1 mmol/L phenylmethylsulfonyl fluoride. The tissue lysate was centrifuged and the supernatant collected. Protein concentration was determined using a bicinchoninic acid protein assay kit (Pierce Chemical Co., Rockford, IL). A 15- g aliquot of protein from each sample was separated on a polyacrylamide gel with 10% sodium dodecyl sulfate. The proteins were subsequently

transferred onto polyvinylidene difluoride membranes (Immobilon®-P membranes; Millipore, Billerica, MA). Membranes were incubated with rabbit immunoglobulin G (IgG) monoclonal antibody to angiotensin type-1 receptor (AT1Rs, 1:1000; Santa Cruz Biotechnology, Santa Cruz, CA), with rabbit IgG polyclonal antibody to β-tubulin (1:1000; Santa Cruz Biotechnology) and with goat IgG polyclonal antibody to phosphorylated-moesin, a substrate of Rho-kinase[11] (p-moesin, 1:1000, Santa Cruz Biotechnology). Membranes were then incubated with horseradish peroxidase-conjugated horse anti-rabbit or anti-goat IgG antibody (1:10,000). β-Tubulin (1:5000; Santa Cruz Biotechnology) was used as an internal control for the brain tissues. Immunoreactivity was detected by enhanced chemiluminescence autoradiography (ECL™ Western blotting detection kit; Amersham Pharmacia Biotech, Uppsala, Sweden), and the film was analyzed using the public domain software NIH Image (developed at the US National Institutes of Health and available on the Internet at http://rsb.info.nih.gov/nih-image/).

Statistical Analysis

All values are expressed as mean ± SE. Analysis of variance was used to compare U-NE and U-E excretion, organ weight, LVDD, LVWT, %FS, and arterial pressure by telemetry system between groups. An unpaired *t*-test was used to compare changes in arterial pressure and heart rate after high-Na ICV infusion, and protein levels between Sham mice and AB mice. Differences were considered to be significant when $P < 0.05$.

References

1. Harada K, Komuro I, Shiojima I, Hayashi D, Kudoh S, Mizuno T, Kijima K, Matsubara H, Sugaya T, Murakami K, Yazaki Y. Pressure overload induces cardiac hypertrophy in angiotensin II type II 1A receptor knockout mice. *Circulation.* 1998;97:1952-1959.
2. Ito K, Kimura Y, Hirooka Y, Sagara Y, Sunagawa K. Activation of Rho-kinase in the brainstem enhances sympathetic drive in mice with heart failure. *Auton Neurosci.* 2008;142:77-81.
3. Cittadini A, Mantzoros CS, Hampton TG, Travers KE, Katz SE, Morgan JP, Flier JS, Douglas PS. Cardiovascular abnormalities in transgenic mice with reduced brown fat: an animal model of human obesity. *Circulation.* 1999;100:2177-2183.
4. Sakai K, Hirooka Y, Shigematsu H, Kishi T, Ito K, Shimokawa H, Takeshita A, Sunagawa K. Overexpression of eNOS in brain stem reduces enhanced sympathetic drive in mice with myocardial infarction. *Am J Physiol Heart Circ Physiol.* 2005;289:H2159-66.
5. Wirth A, Benyó Z, Lukasova M, Leutgeb B, Wettschureck N, Gorbey S, Örsy P, Horváth B, Maser-Gluth C, Greiner E, Lemmer B, Schütz G, Gutkind S, Offermanns S. G_{12}-G_{13}-LARG-mediated signaling in vascular smooth muscle is required for salt-induced hypertension.
6. Rahmouni K, Haynes WG, Morgan DA, Mark AL. Selective resistance to central neural administration of leptin in agouti obese mice. *Hypertension.* 2002;39:486-490.
7. Lu N, Helwig BG, Fels RJ, Parimi S, Kenney MJ. Central tempol alters basal sympathetic nerve discharge and attenuates sympathetic excitation to central ANGII. *Am J Physiol.* 2004;287:H2626-H2633.
8. Wang N, Jiang CL, Wang CY, Yao QY. Role of brain angiotensin AT1 receptor in the

carbachol-induced natriuresis and expression of nNOS in the locus coeruleus and proximal convoluted tubule. *Physiol Res*. 2007;56:383-391

9. Huang BS, Leenen FHH. Blockade of brain mineralcorticoid receptors or Na^+ channels prevents sympathetic hyperactivity and improve cardiac function in rats post-MI. *Am J Physiol.* 2005;288:H2491-H2497.
10. Uehata M, Ishizaki T, Satoh H, Ono T, Kawahara T, Morishita T, Tamakawa H, Yamagami K, Inui J, Maekawa M, Narumiya S. Calcium sensitization of smooth muscle mediated by a Rho-associated protein kinase in hypertension. *Nature.* 1997;389:990-994.
11. Matsui T, Maeda M, Doi Y, Yonemura S, Amano M, Kaibuchi K, Tsukita S. Rho-kinase phosphorylate COOH-terminal threonines of ezrin/radixin/moesin (ERM) proteins and regulates their head-to-tail association. *J Cell Biol.* 1998;140:647-657.

Online Table I LVEDP for Each Group

Group	LVEDP (mmHg)
Sham- 4	7.0 ± 0.8
Sham-R	9.6 ± 0.2
AB-4	13.5 ± 1.6 *
AB-R	13.3 ± 1.1
AB-H	18.6 ± 0.8 #

n=4 for each, *P<0.05 versus Sham-4, #P<0.05 versus Sham-R

Online Table II MAP and HR for Each Group

Group (Number)	MAP (mmHg)	HR (bpm)
Sham- 4 (8)	87 ± 2	388 ± 9
Sham-R (5)	88 ± 2	390 ± 5
Sham-H (5)	95 ± 3	401 ± 6
AB-4 (8)	107 ± 4 *	429 ± 28 *
AB-R (5)	94 ± 3	460 ± 14 $^{\#}$
AB-H (5)	80 ± 5	497 ± 3 $^{\#,+}$
AB-H 1w (5)	123 ± 7	490 ± 15 *
AB-HB (4)	95 ± 5	435 ± 17 $^{\$}$
AB-HY (5)	94 ± 3	372 ± 15 $^{\$}$
AB-HT (4)	88 ± 1	402 ± 6 $^{\$}$
AB-4 (FA) (6)	92 ± 4	

*$P<0.05$ versus Sham-4, $^{\#}P<0.05$ versus Sham-R, $^{+}P<0.05$ versus AB-R

$^{\$}P<0.05$ versus AB-H

FA measured from femoral artery.

Online Figure I

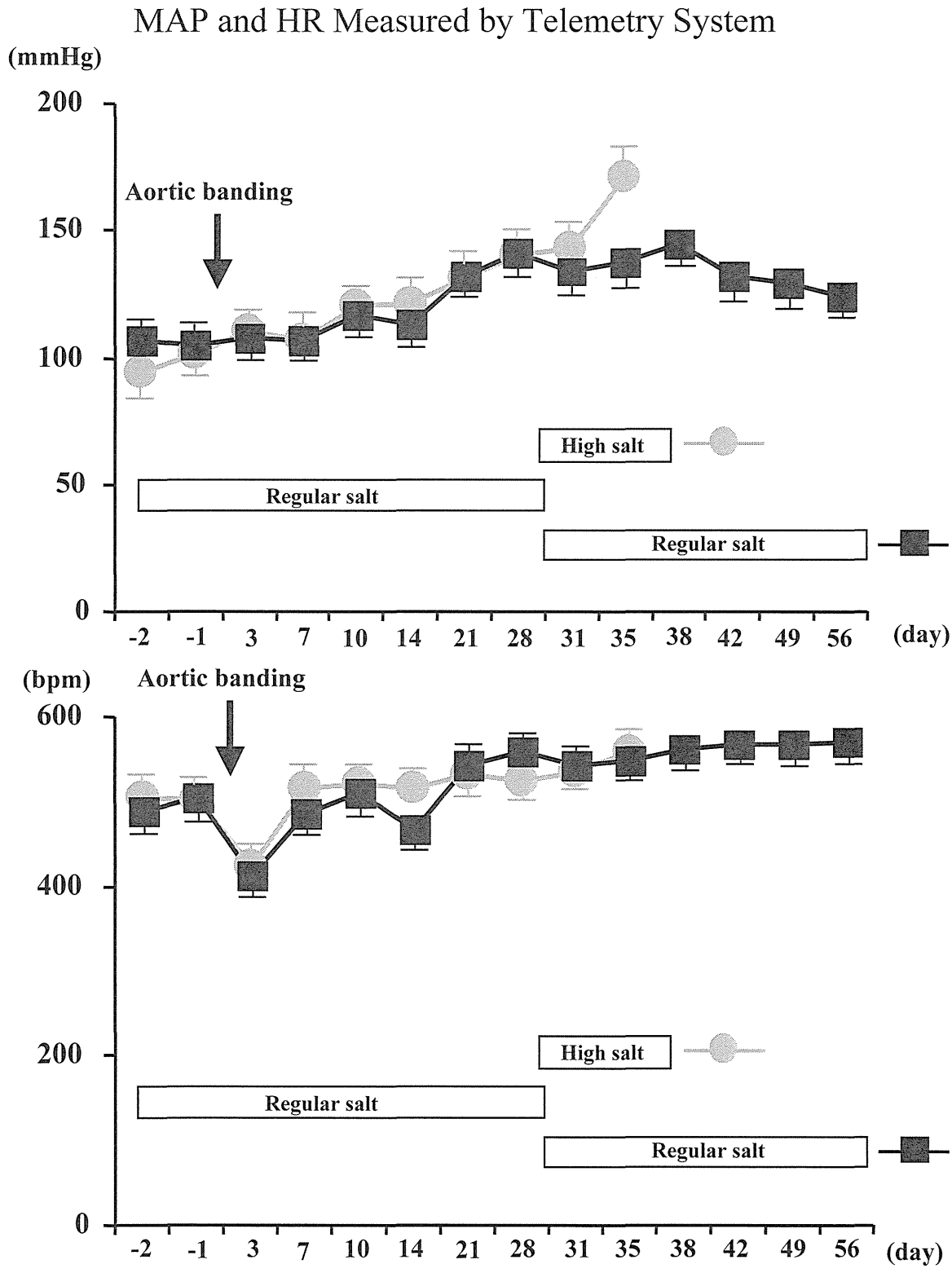

Online Figure I: Graphs showing mean arterial pressure (MAP) (upper panel) and heart rate (HR) (lower panel) measured by telemetry before and after aortic banding (arrow). Circles indicate the data from mice fed a high salt diet and squares indicate the data from mice fed a regular salt diet. Please see details in the Results section of the text.

Circ J 2009; **73:** 851–859

Servo-Controlled Hind-Limb Electrical Stimulation for Short-Term Arterial Pressure Control

Toru Kawada, MD; Shuji Shimizu, MD; Hiromi Yamamoto, MD*;
Toshiaki Shishido, MD; Atsunori Kamiya, MD; Tadayoshi Miyamoto, PhD**;
Kenji Sunagawa, MD†; Masaru Sugimachi, MD

Background: Autonomic neural intervention is a promising tool for modulating the circulatory system thereby treating some cardiovascular diseases.

Methods and Results: In 8 pentobarbital-anesthetized cats, it was examined whether the arterial pressure (AP) could be controlled by acupuncture-like hind-limb electrical stimulation (HES). With a 0.5-ms pulse width, HES monotonically reduced AP as the stimulus current increased from 1 to 5 mA, suggesting that the stimulus current could be a primary control variable. In contrast, the depressor effect of HES showed a nadir approximately 10 Hz in the frequency range between 1 and 100 Hz. Dynamic characteristics of the AP response to HES approximated a second-order low-pass filter with dead time (gain: −10.2±1.6 mmHg/mA, natural frequency: 0.040±0.004 Hz, damping ratio 1.80±0.24, dead time: 1.38±0.13 s, mean±SE). Based on these dynamic characteristics, a servo-controlled HES system was developed. When a target AP value was set at 20 mmHg below the baseline AP, the time required for the AP response to reach 90% of the target level was 38±10 s. The steady-state error between the measured and target AP values was 1.3±0.1 mmHg.

Conclusions: Autonomic neural intervention by acupuncture-like HES might provide an additional modality to quantitatively control the circulatory system. (*Circ J* 2009; **73:** 851–859)

Key Words: Proportional-integral controller; Transfer function

Because abnormality in the autonomic nervous system is often associated with cardiovascular diseases, treating cardiovascular diseases by autonomic neural interventions have attracted many researchers![1–6] Recently, autonomic neural interventions using electronic devices have again gained the focus of attention as a potential modality for treating cardiovascular diseases resistant to conventional therapeutics. To name a few, chronic vagal nerve stimulation dramatically improves the survival of chronic heart failure after myocardial infarction in rats![7] Chronic baroreceptor activation enhances the survival of pacing-induced heart failure in dogs![8] A recent version of a device-based treatment of hypertension in human is reported![9] A framework of electrical neural intervention is also effective to elevate arterial pressure (AP) against hypotensive events![10–13]

Aside from direct neural stimulation, electroacupuncture can modify autonomic balance, thereby treating cardiovascular diseases![4–16] Although one feature of the electroacupuncture might be its long-lasting effects, immediate cardiovascular responses to acupuncture-like stimulation are also observed in several experimental settings. For example, a 60-s manual acupuncture-like stimulation of a hind limb reduces renal or cardiac sympathetic nerve activity, causing hypotension and bradycardia in anesthetized rats![17,18] We have shown that electrical stimulation of a hind limb using acupuncture needles immediately resets the arterial baroreflex and reduces sympathetic nerve activity in anesthetized rabbits![19] Acupuncture-like hind-limb electrical stimulation (HES) induces immediate hypotension with changes in the relationship between cardiac and renal sympathetic nerve activities in anesthetized cats![20]

In the present study, we hypothesized that AP could be controlled by HES. Quantification of the dynamic input–output relationship between a given stimulus and the AP response is essential for artificially controlling AP![10–12] Accordingly, the first aim was to identify the dynamic input–output relationship between HES and the AP response. The second aim was to develop a feedback controller system that could reduce AP at a prescribed target level using HES.

(Received November 17, 2008; revised manuscript received December 10, 2008; accepted December 21, 2008; released online March 18, 2009)

*Department of Cardiovascular Dynamics, Advanced Medical Engineering Center, National Cardiovascular Center Research Institute, Suita, *Division of Cardiology, Department of Internal Medicine, Kinki University School of Medicine, Osakasayama, **Department of Physical Therapy, Faculty of Health Sciences, Morinomiya University of Medical Sciences, Osaka and †Department of Cardiovascular Medicine, Graduate School of Medical Sciences, Kyushu University, Fukuoka, Japan*

Mailing address: Toru Kawada, MD, Department of Cardiovascular Dynamics, Advanced Medical Engineering Center, National Cardiovascular Center Research Institute, 5-7-1 Fujishirodai, Suita 565-8565, Japan. E-mail torukawa@res.ncvc.go.jp

Methods

Surgical Preparation

Animal care was provided in strict accordance with the *Guiding Principles for the Care and Use of Animals in the Field of Physiological Sciences,* approved by the Physiological Society of Japan. All protocols were approved by the Animal Subject Committee of the National Cardiovascular Center. Eight adult cats weighing from 2.3 to 4.3 kg were

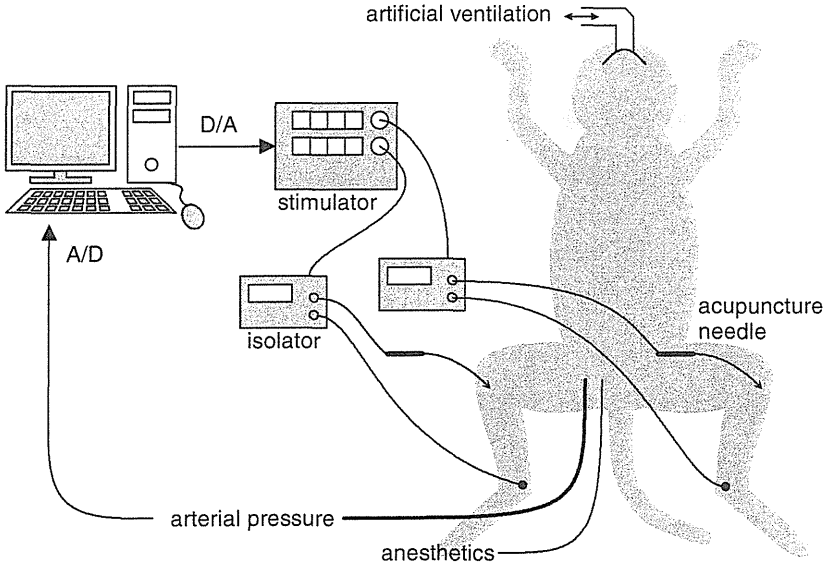

Figure 1. Experimental setup.

anesthetized by an intraperitoneal injection of pentobarbital sodium (30–35 mg/kg) and ventilated mechanically via a tracheal tube with oxygen-supplied room air. The depth of anesthesia was maintained with a continuous intravenous infusion of pentobarbital sodium (1–2 mg·kg^{-1}·h^{-1}) through a catheter inserted into the right femoral vein. Vecuronium bromide (0.5–1.0 mg·kg^{-1}·h^{-1}, iv) was given continuously to suppress muscular activity. AP was measured using a catheter-tip manometer inserted from the right femoral artery and advanced into the thoracic aorta.

HES

In the supine position, both hind limbs were lifted to obtain a better view of the lateral sides of the lower legs. An acupuncture needle with a diameter of 0.2 mm (CE0123, Seirin-Kasei, Shimizu, Japan) was inserted into a point below the knee joint just lateral to the tibia[20] A 23-gauge needle was inserted into the skin behind the ankle as the ground. HES was applied bilaterally via 2 independent isolators connected to an electrical stimulator (SEN 7203, Nihon Kohden, Tokyo, Japan) as shown in **Figure 1**. The pulse width was changed manually whereas the stimulus frequency and the stimulus current were controlled by a dedicated laboratory computer system. The electrical stimulation was started after the hemodynamic effects of needle insertion had disappeared, and the acupuncture needle remained inserted during each protocol.

Protocols

Protocol 1 (n=8) To quantify the AP response to HES as a function of stimulus current and pulse width, we fixed the stimulus frequency at 10 Hz and changed the stimulus current stepwise from 0 to 5 mA in 1-mA increments every minute. The 6-min current test was repeated with an intervening interval of 3–5 min using different pulse widths (0.1, 0.2, 0.5 and 1 ms). The order of the pulse-width settings was randomized across the animals.

Protocol 2 (n=8) To quantify the AP response to HES as a function of stimulus frequency and pulse width, we fixed the stimulus current at 3 mA and changed the stimulus frequency sequentially from 0 to 100 Hz (0, 1, 2, 5, 10, 15, 20, 50 and 100 Hz). Each stimulus frequency was maintained for 1 min. The 9-min frequency test was repeated with an intervening interval of 3–5 min using different pulse widths (0.1, 0.2, 0.5 and 1 ms). The order of the pulse-width settings was randomized across the animals.

Protocol 3 (n=8) To identify the dynamic input–output relationship between HES and the AP response, we randomly turned HES on and off every 2 s according to a binary white noise sequence for 30 min. The HES setting (0.5-ms pulse width, 10 Hz, 3 mA) was chosen to induce effective hypotension based on the preliminary results obtained from Protocols 1 and 2.

Protocol 4 (n=8) Based on the result of Protocol 3, we designed a feedback controller that could automatically adjust the stimulus frequency and the stimulus current for HES. The pulse width was fixed at 0.5 ms. To examine the performance of the feedback controller, we set a target AP value at 20 mmHg below the baseline AP and activated the feedback controller for 10 min.

The following 2 supplemental protocols were performed in 3 of the 8 cats: (1) we inserted 2 acupuncture needles into the triceps surae muscle with a distance of approximately 2.5 cm, and examined if changes in AP was associated with direct muscle stimulation (0.5-ms pulse width, 10 Hz, 3 mA). Both hind limbs were stimulated simultaneously using 2 independent isolators; and (2) we exposed the sciatic nerve after finishing Protocols 1 through 4, and examined if sectioning the sciatic nerve abolished the hemodynamic effects of HES. Unilateral HES was performed (0.5-ms pulse width, 10 Hz, 3 mA) before and after sectioning the ipsilateral sciatic nerve.

Data Analysis

In Protocols 1 and 2, the AP value was obtained by averaging the last 10-s data at each stimulus condition. In Protocol 1, the effect of stimulus current was assessed by changes in AP from the 0-mA stimulus condition for each pulse width. In Protocol 2, the effect of stimulus frequency was assessed by changes in AP from the 0-Hz stimulus condition for each pulse width.

In Protocol 3, the transfer function from HES to AP was estimated by means of an analysis for one-input, one-output systems. Data were first resampled at 10 Hz and segmented into 8 sets of 50%-overlapping bins of 4,096 points each. For each segment, a linear trend was subtracted and a

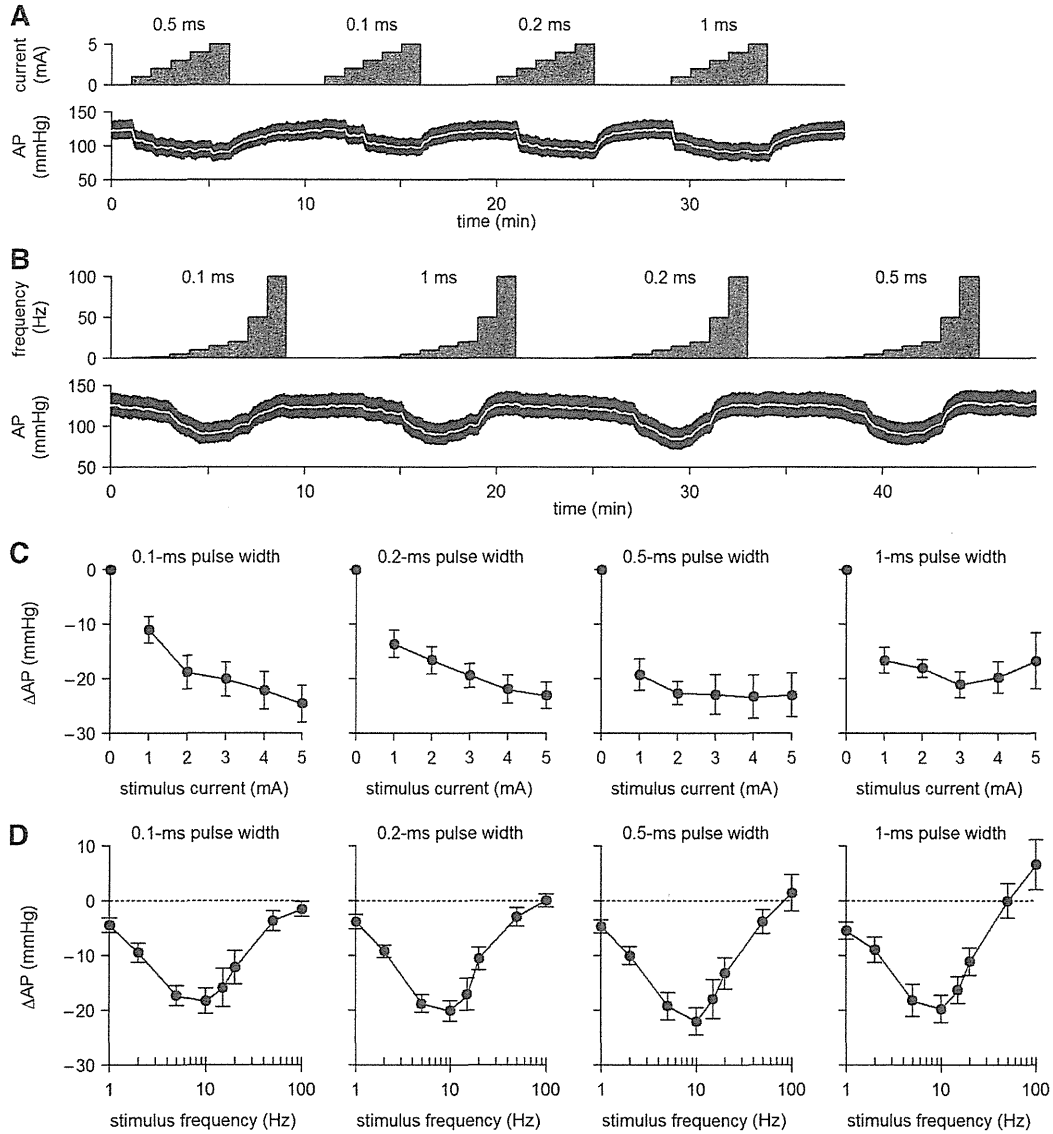

Figure 2. (**A**) Typical recordings of Protocol 1 showing the effects of stimulus current and pulse width on arterial pressure (AP). (**B**) Typical recordings of Protocol 2 showing the effects of stimulus frequency and pulse width on AP. The white lines in the AP traces indicate 2-s moving averaged data. (**C**) Changes in AP as a function of the stimulus current. AP decreased monotonously as the stimulus current increased ($P<0.05$). (**D**) Changes in AP as a function of the stimulus frequency. AP decreased more as the stimulus frequency increased from 1 to 10 Hz but the depressor effect became smaller when the stimulus frequency exceeded 10 Hz ($P<0.05$).

Hanning window was applied. Frequency spectra of the input and output were obtained via fast Fourier transformation. Next, the ensemble averages of input power spectral density [$S_{XX}(f)$], output power spectral density [$S_{YY}(f)$], and cross spectral density between the input and output [$S_{YX}(f)$] were calculated over the 8 segments. Finally, the transfer function from input to output [$H(f)$] was calculated as:[21]

$$H(f)=\frac{S_{YX}(f)}{S_{XX}(f)} \quad (1)$$

To quantify the linear dependence between the input and output signals in the frequency domain, a magnitude-squared coherence function [$Coh(f)$] was also calculated as:[21]

$$Coh(f)=\frac{|S_{YX}(f)|^2}{S_{XX}(f)S_{YY}(f)} \quad (2)$$

In Protocol 4, the performance of the feedback controller was evaluated by the time required for the AP response to reach 90% of the target AP decrease and by the standard deviation of the steady-state error between the target and measured AP values during the last 5 min of the 10-min feedback control. These 2 values were calculated based on the 2-s moving averaged data of AP.

Statistical Analysis

All data are presented as mean and SE values. In Protocol 1, changes in AP were examined by 2-way repeated-measures analysis of variance (ANOVA) using the stimulus current as one factor and the pulse width as the other factor?[22] In Protocol 2, changes in AP were examined by 2-way repeated-measures ANOVA using the stimulus frequency as one factor and the pulse width as the other factor. Differences were considered significant when $P<0.05$.

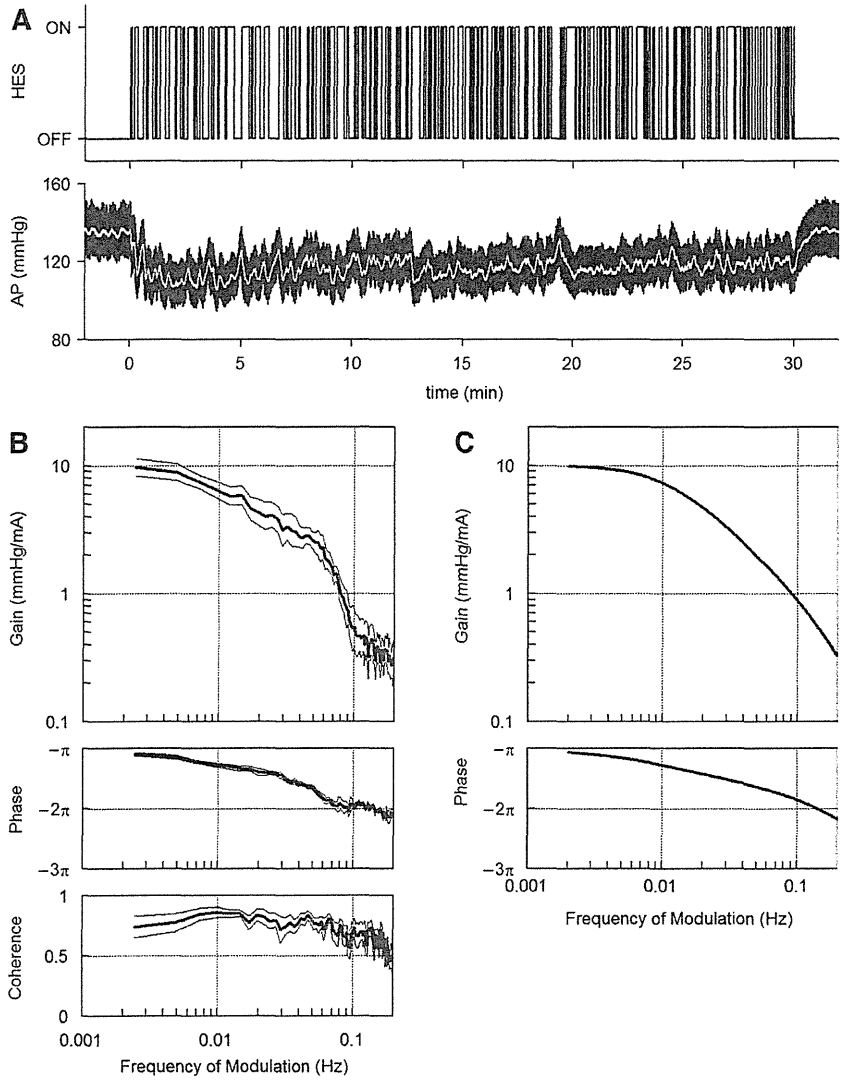

Figure 3. (**A**) Typical recordings of random hind-limb electrical stimulation (HES) and arterial pressure (AP) response. (**B**) Transfer function from HES to the AP response averaged from 8 cats. Thick and thin lines indicate mean and mean±SE values, respectively. (**C**) A model transfer function of the second-order low-pass filter with a lag time that mimics the transfer function from HES to AP.

Results

Relationship Between Stimulus Intensity and AP Response

Typical time series of Protocols 1 and 2 obtained from one animal are shown in **Figures 2A** and **B**, respectively. The pulse width was set in a random order. In Protocol 1, baseline AP obtained at the 0-mA stimulus condition was 118.4±5.4 mmHg across the animals. Changes in mean AP as a function of stimulus current are summarized in **Figure 2C**. The decrease in AP became greater as the stimulus current increased. The overall statistical analysis indicated that the effect of the stimulus current on the magnitude of AP decrease was significant whereas that of pulse width was not. There was no significant interaction effect between the stimulus current and the pulse width.

In Protocol 2, baseline AP at the 0-Hz stimulus condition was 117.6±5.9 mmHg across the animals. Changes in mean AP as a function of stimulus frequency are summarized in **Figure 2D**. The decrease in AP became greater as the stimulus frequency increased from 1 to 10 Hz but it became smaller when the stimulus frequency exceeded 10 Hz. At the pulse width of 1 ms, the stimulus frequency of 100 Hz even increased AP. The overall statistical analysis indicated that the effect of stimulus frequency on the magnitude of AP decrease was significant whereas that of pulse width was not. There was no significant interaction effect between the stimulus frequency and the pulse width.

Dynamic Characteristics of AP Response to HES

Figure 3A depicts a typical time series obtained from Protocol 3. HES was turned on and off randomly, which decreased the mean level of AP and also caused intermittent AP variations. When HES was finally turned off at 30 min, AP began to increase toward the prestimulation value. A long-lasting effect of HES was not observed in the present protocol. The white line in the AP trace represents the 2-s moving averaged data of AP.

The results of transfer function analysis are depicted in **Figure 3B**. In the gain plot, the magnitude of AP response relative to the HES input was plotted in the frequency domain. The gain value became smaller as the frequency increased, indicating the low-pass characteristics of the AP response to HES. In the phase plot, AP showed an out-of-phase relationship with HES at the lowest frequency (0.0024 Hz). The phase delayed more with increasing the frequency of modulation. The coherence value was approximately 0.7 in the frequency range below 0.06 Hz. The

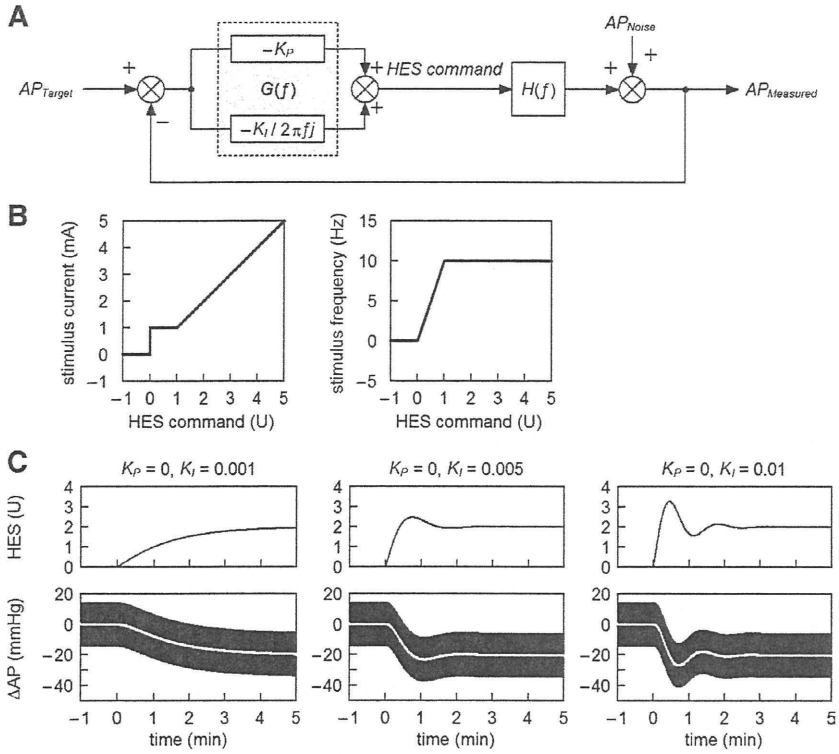

Figure 4. (**A**) A simplified diagram of the feedback controller utilized in the present study. AP_{Target}: target arterial pressure (AP); AP_{Noise}: noise in AP in terms of the control theory; $AP_{Measured}$: measured AP; $G(f)$: transfer function of the controller; $H(f)$: transfer function from hind-limb electrical stimulation (HES) to the AP response; K_P: proportional gain; K_I: integral gain; f and j denote the frequency and imaginary unit, respectively (see Appendix A for details). (**B**) Functions that convert the HES command into the stimulus current and the stimulus frequency. (**C**) Simulation results showing the feedback control of AP by HES. At time zero, the target AP was set at −20 mmHg. In the simulation, a sinusoidal wave (3 Hz, 15 mmHg in amplitude) was added to mimic the pulse pressure in AP. White lines indicate the 2-s moving averaged data of the simulated AP response.

coherence value became smaller in the frequency range above 0.1 Hz but still retained a value of 0.5, indicating that approximately half of the AP variation was explained by the HES input.

The general feature of the dynamic characteristics of the AP response to HES approximated what is known as a second order low-pass filter with a pure dead time, which is mathematically described as:

$$H(f)=\frac{-K}{1+2\zeta\frac{f}{f_N}j+\left(\frac{f}{f_N}j\right)^2}\exp(-2\pi fjL) \quad (3)$$

where K is the steady-state gain, f_N is the natural frequency, ζ is the damping ratio, and L is the pure dead time. When we performed an iterative non-linear least square fitting using a downhill Simplex method, K, f_N, ζ and L were estimated as 10.2±1.6 mmHg/mA, 0.040±0.004 Hz, 1.80±0.24 and 1.38±0.13 s, respectively. A model transfer function shown in **Figure 3C** was drawn using K, f_N, ζ and L of 10 mmHg/mA, 0.04 Hz, 2 and 1 s, respectively.

Development of a Feedback Controller

We used a classical feedback controller to adjust the stimulus intensity of HES[23–25] In reference to **Figure 4A**, a HES command is determined based on a difference between measured and target AP values. $G(f)$ represents the transfer function of the controller with a proportional gain (K_P) and an integral gain (K_I). $H(f)$ indicates the model transfer function shown in **Figure 3C**. A detailed mathematical description of the controller is supplied in Appendix A.

To circumvent a threshold phenomenon in the stimulus current-AP response relationship (see Appendix B for details), the HES command (in an arbitrary unit) was transformed into the stimulus current (in mA) by a factor of 1 (**Figure 4B, Left**) only when the HES command exceeded unity. When the HES command was less than unity, the stimulus current was held at 1 mA and the HES command was transformed into the stimulus frequency (in Hz) by a factor of 10 (**Figure 4B, Right**). The stimulation was turned off when the HES command became negative.

Several sets of simulations were conducted using the model transfer function. The target AP was set at 20 mmHg below the baseline AP. To mimic the pulse pressure in AP, a 3-Hz sinusoidal wave (corresponding to the HR of 180 beats/min) with an amplitude of 15 mmHg (corresponding to the pulse pressure of 30 mmHg) was added to the AP signal. To avoid pulsatile variation in the HES command, we set the proportional gain at zero. Under this condition, when the integral gain was set at 0.001, AP decreased gradually and it took more than 3 min to reach the target AP (**Figure 4C, Left**). When the integral gain was set at 0.005, AP decreased more promptly and reached the target AP in less than 1 min (**Figure 4C, Center**). When the integral gain was set at 0.01, the AP response occurred more rapidly but showed significant oscillations before settling (**Figure 4C, Right**). Based on these simulation results, we set the proportional gain at zero and the integral gain at 0.005 for the actual feedback-control experiment in Protocol 4.

Performance of the Feedback Controller

Figure 5A demonstrates the AP regulation by HES obtained from 2 typical animals. The proportional and integral gains of the controller were not altered among the animals (ie, K_P=0, K_I=0.005). The white line in the AP trace indicates 2-s moving averaged data. The target AP was set at 20 mmHg below the AP value just before the application of HES. The feedback controller was activated for 10 min, which decreased AP at the target level. The HES command was individualized via the feedback mechanism. In the left panel of **Figure 5A**, the HES command gradually increased throughout the 10-min regulation. In the right panel of **Figure 5A**, the HES command was less than unity